Towards the molecular architecture of the peroxisomal receptor docking complex

Pascal Lill[a,1], Tobias Hansen[b,1], Daniel Wendscheck[c,1], Bjoern Udo Klink[a], Tomasz Jeziorek[b], Dimitrios Vismpas[a], Jonas Miehling[a], Julian Bender[c,2], Andreas Schummer[c,3], Friedel Drepper[c,d], Wolfgang Girzalsky[b], Bettina Warscheid[c,d,4], Ralf Erdmann[b,4], and Christos Gatsogiannis[a,e,4]

[a]Department of Structural Biochemistry, Max Planck Institute of Molecular Physiology, 44227 Dortmund, Germany; [b]Institute of Biochemistry and Pathobiochemistry, Faculty of Medicine, System Biochemistry, Ruhr University Bochum, 44801 Bochum, Germany; [c]Biochemistry and Functional Proteomics, Institute of Biology II, Faculty of Biology, University of Freiburg, 79104 Freiburg, Germany; [d]Signalling Research Centres BIOSS and CIBSS, University of Freiburg, 79104 Freiburg, Germany; and [e]Institute for Medical Physics and Biophysics and Center for Soft Nanoscience, Westfälische Wilhelms Universität Münster, 48149 Münster, Germany

Edited by James H. Hurley, University of California, Berkeley, CA, and approved October 19, 2020 (received for review May 16, 2020)

Import of yeast peroxisomal matrix proteins is initiated by cytosolic receptors, which specifically recognize and bind the respective cargo proteins. At the peroxisomal membrane, the cargo-loaded receptor interacts with the docking protein Pex14p that is tightly associated with Pex17p. Previous data suggest that this interaction triggers the formation of an import pore for further translocation of the cargo. The mechanistic principles, however, are unclear, mainly because structures of higher-order assemblies are still lacking. Here, using an integrative approach, we provide the structural characterization of the major components of the peroxisomal docking complex Pex14p/Pex17p, in a native bilayer environment, and reveal its subunit organization. Our data show that three copies of Pex14p and a single copy of Pex17p assemble to form a 20-nm rod-like particle. The different subunits are arranged in a parallel manner, showing interactions along their complete sequences and providing receptor binding sites on both membrane sides. The long rod facing the cytosol is mainly formed by the predicted coiled-coil domains of Pex14p and Pex17p, possibly providing the necessary structural support for the formation of the import pore. Further implications of Pex14p/Pex17p for formation of the peroxisomal translocon are discussed.

peroxisomal import | peroxin | docking complex | peroxisomal translocon | cryoEM

Peroxisomes are organelles present nearly ubiquitously in eukaryotic cells, ranging from unicellular yeasts to multicellular organisms, such as plants and humans. Beside β-oxidation of fatty acids as a main conserved function of peroxisomes, a broad range of additional metabolic functions is linked to this organelle, underscored by severe and frequently lethal phenotypes of human disorders (1, 2). These organelles do not contain DNA and thus all peroxisomal matrix proteins are encoded in the nucleus and synthesized on free polyribosomes in the cytosol. Subsequently, matrix proteins are targeted to the organelle by peroxisomal import receptors (3). A remarkable feature of peroxisomes is that unlike the transport of unfolded polypeptides across the membranes of the endoplasmic reticulum and mitochondria, they can import already folded, cofactor-bound, and even oligomeric proteins (4, 5). This transport is highly selective and mediated by specific import sequences known as peroxisomal targeting signals (PTSs) (6, 7). Peroxisomal matrix proteins equipped with either a carboxyl-terminal PTS1 or an amino-terminal PTS2, are recognized and bound in the cytosol by the import receptor Pex5p or Pex7p, respectively (8, 9). A peroxisomal membrane-associated complex consisting of Pex13p, Pex14p, and Pex17p in yeast allows docking of the cargo-loaded receptor (10–14). This primary interaction of the cargo-loaded receptor with the docking complex induces the formation of a transient and highly dynamic import pore, necessary for the translocation of the cargo across the peroxisomal membrane (15–17). How translocation and release of the cargo are realized in detail still remains enigmatic but it has been previously shown that the receptor is exported from the peroxisomal membrane in an ubiquitin- and ATP-dependent manner, a process that is discussed to provide the driving force for cargo import according to the export-driven import model (18–20).

The receptor–docking complex is of major importance for peroxisomal matrix protein import, as it provides a binding platform for newly formed receptor–cargo complexes at the peroxisomal membrane. Both Pex13p and Pex14p are peroxisomal membrane proteins providing several binding sites for the import receptors Pex5p and Pex7p (16). Docking of the Pex5p–PTS1 protein complex at the peroxisome membrane is supposed to occur at Pex14p (21, 22). Pex17p is tightly associated with Pex14p (23), but its precise function remains unknown. Although Pex17p is part of the docking complex in yeast, it does not significantly contribute to the assembly of the Pex13p/Pex14p subcomplex (15, 23, 24), and its counterpart in higher eukaryotes

Significance

Peroxisomal matrix enzymes are synthesized in the cytosol and carry targeting signals. These are recognized and bound by an import receptor in the cytosol. The cargo-loaded receptor further binds to the "docking" complex at the peroxisomal membrane. The docking events are expected to trigger the formation of a transient pore allowing import of the cargo into the peroxisomal matrix. Here using cryoelectron microscopy complemented by native MS, cross-linking MS, SEC MALS, and immunogold labeling, we provide the structural characterization of the major components of the yeast peroxisomal docking complex. Pex14p/Pex17p assemble in a parallel 3:1 bundle arrangement to form intriguingly long flexible rods that emanate into the cytosol to recruit the cargo-loaded receptor for further translocation events.

Author contributions: B.W., R.E., and C.G. designed research; P.L., T.H., D.W., B.U.K., T.J., D.V., J.M., J.B., A.S., F.D., W.G., and C.G. performed research; P.L., T.H., D.W., B.U.K., T.J., J.B., F.D., W.G., and C.G. analyzed data; and B.W., R.E., and C.G. wrote the paper.

The authors declare no competing interest.

This article is a PNAS Direct Submission.

[1]P.L., T.H., and D.W. contributed equally to this work.

[2]Present address: Interdisciplinary Research Center HALOmem, Institute for Biochemistry and Biotechnology, Martin Luther University Halle-Wittenberg, 06120 Halle (Saale), Germany.

[3]Present address: Protagen Protein Services GmbH, 74076 Heilbronn, Germany.

[4]To whom correspondence may be addressed. Email: bettina.warscheid@biologie.uni-freiburg.de, Ralf.Erdmann@rub.de, or christos.gatsogiannis@uni-muenster.de.

This article contains supporting information online at https://www.pnas.org/lookup/suppl/doi:10.1073/pnas.2009502117/-/DCSupplemental.

First published December 15, 2020.

has not yet been identified. However, Pex17p is essential for peroxisomal import of both PTS1 and PTS2 proteins (14). Strikingly, both import receptors, Pex5p and Pex7p, associate with the docking complex (Pex13p/Pex14p) in absence of Pex17p, but with decreased efficiency (24).

Furthermore, albeit a close association between the core components of the docking complex (Pex13p/Pex14p) is important for matrix protein import (25), there are several lines of evidence that Pex13p is not a permanent component of the peroxisomal docking complex or the import pore (10, 26) and interestingly, an assembly between the receptor Pex5p and the docking component Pex14p in absence of Pex13p is capable per se of forming a large transient channel at the peroxisome membrane (15).

However, little is known about the molecular mechanism underlying the primary docking and subsequent translocation events, largely because structures of the higher-order assemblies are not available. Here, using cryo-electron microscopy single particle analysis (cryoEM SPA) and cryo-electron tomography (cryoET) combined with cross-linking and native mass spectrometry (MS), we set out to characterize the overall architecture of the yeast Pex14p/Pex17p complex.

Results

Pex14p Forms a 3:1 Heterotetrameric Complex with Pex17p. Yeast Pex14p consists of three structural regions: a highly conserved N-terminal region containing a putative transmembrane domain (TMD), a long and a short coiled-coil domain in the middle region, and an unstructured C-terminal domain (Fig. 1*A*). Yeast Pex14p contains two separated binding sites for the PTS1 import receptor Pex5p, localized at its N and C termini (Fig. 1*A*) (27). Mammalian PEX14 contains a putative transmembrane segment but only one PEX5 binding site at the N-terminal region of the protein, and only a single, shortened central predicted coiled-coil domain, which has been shown to mediate dimerization, whereas the transmembrane domain is responsible for formation of higher-order assemblies (28, 29). The N-terminal region of Pex14p is highly conserved among species. This region binds Pex5p via *WXXX(F/Y)* motifs that are located in the N-terminal domain of Pex5p (30–32). These *WXXX(F/Y)* motifs are typical sequence features of Pex5p but their number varies, two are present in yeast, eight in human PEX5 (30, 33). The Pex5p interface for binding to the C-terminal region of yeast Pex14p is still unknown.

The topology of Pex14p at the peroxisomal membrane has been controversial when discussed, but recent protease-protection studies suggest a N_{in}-C_{out} membrane topology (34). Pex17p contains a putative TMD near the N terminus and two short coiled-coil domains (Fig. 1*A*). Pex14p and Pex17p associate together to form a tight core complex that contains an excess of Pex14p over Pex17p (23). The oligomeric composition of this complex is, however, unknown. Interestingly in rice blast fungus *Magnaporthe*, Pex14p and Pex17p fuse to form a unique Pex14p/Pex17p (or Pex33p) peroxin (35). Here, we first coexpressed yeast $Strep_{II}$-Pex14p and His_6-Pex17p in *Escherichia coli* (*SI Appendix*). Initial experiments revealed a dominant protein band of about 35 kDa, which represents a truncated Pex14p variant starting at the methionine at position 51, as identified by MS (*SI Appendix*, Fig. S1 *A–C*). The reason for the appearance of such a Pex14p variant might be either an alternative translation start or a site-specific degradation. However, a methionine at this position is not conserved among species (28) and such a Pex14p variant was not observed in whole cell lysates of yeast (10, 23). Along this line, replacement of Met51 by leucine and expression of this Pex14p variant did result in functional complementation of the growth defect of the corresponding *pex14Δ* mutant on oleic acid as a single carbon source and recovery of protein import into peroxisomes (*SI Appendix*, Fig. S2). Accordingly,

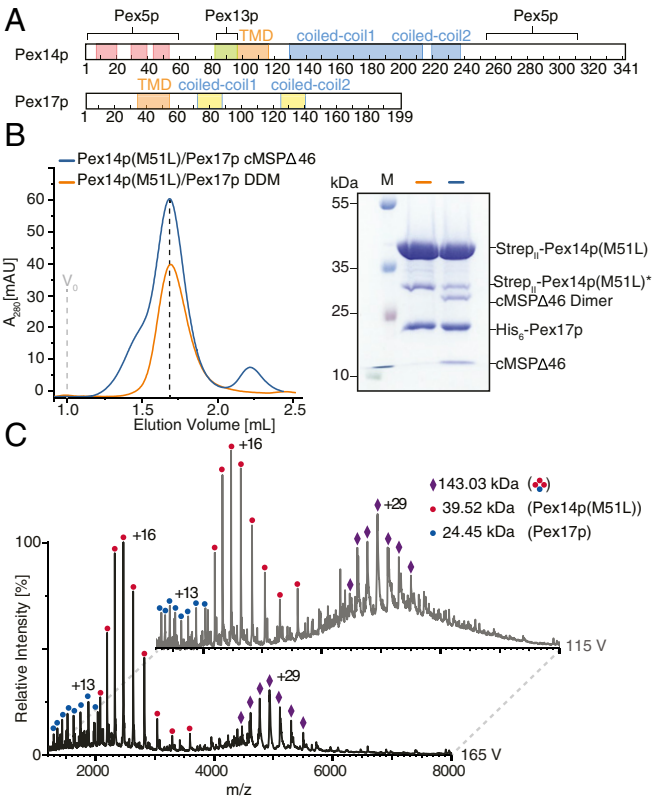

Fig. 1. Molecular composition of Pex14p/Pex17p. (*A*) Primary domain structure of yeast Pex14p and Pex17p. Red: alpha-helix; orange: predicted membrane domain (TMD), blue: predicted coiled-coil domain of Pex14p; yellow: predicted coiled-coil domain of Pex17p; pale green: Pex13p binding domain. Binding sites to the peroxisomal receptor Pex5p are also indicated. (*B*) Size exclusion chromatography of recombinant $Strep_{II}$-Pex14p(M51L)/His_6-Pex17p in DDM (n-Dodecyl β-D-maltoside) (orange) and cMSP1D1Δ4 to 6 nanodiscs (blue), using a Superose 6 increase column 5/150 with a column volume of 3 mL. The dashed line indicates the fraction of the Pex14p/Pex17p peak used for subsequent EM studies. The SDS/PAGE of the respective EM sample is shown. (*C*) Native MS spectra of recombinant $Strep_{II}$-Pex14p(M51L)/His_6-Pex17p in 200 mM ammonium acetate, pH 6.8, 0.015% DDM recorded at two different accelerating potentials (115 V, *Top* spectrum; 165 V, *Bottom* spectrum) for transfer into the collision cell. Peak series assigned to series of charge states are annotated by symbols as shown in the legend. At a lower acceleration voltage of 115 V for collisional activation (gray spectrum), a charge state series of the complex in the *m/z* range 5,000 to 6,000 was partly resolved. Charge state series in the lower *m/z* region indicate masses of monomeric Pex14p and Pex17p. The series at *m/z* ~5,000 indicates a mass of 143.03 kDa corresponding to a subunit stoichiometry of 3:1 of Pex14p:Pex17p as schematically depicted in the legend. Increase of the applied collisional energy from 115 V to 165 V allowed the effective removal of detergent and buffer molecule adducts and thereby peak sharpening.

Met51 is not required for the function of Pex14p in peroxisome biogenesis. When expressing Pex14p(M51L) in *E. coli*, the additional band at 35 kDa almost disappeared (*SI Appendix*, Fig. S1 *D* and *E*). The Pex14p(M51L)/Pex17p complex was then purified by a two-step affinity chromatography (Strep-Tactin and nickel-nitrilotriacetic acid [Ni-NTA] affinity chromatography) and size-exclusion chromatography (SEC) in presence of DDM (n-dodecyl-β-D-maltosid) (Fig. 1*B* and *SI Appendix*, Fig. S3*A*).

To investigate the composition of the complex, we then used native MS preserving noncovalent interactions during transfer into the gas phase. Collisional activation produced a well-resolved peak series, indicating the removal of the protein-bound detergent (Fig. 1*C*) (36). The two prominent charge state series can be assigned to molecular masses of 39.52 kDa,

corresponding to monomeric Pex14p, and 143 kDa, indicating a 3:1 complex of Pex14p:Pex17p. A minor series can be attributed to monomeric Pex17p with a mass of 24.45 kDa. The subunit stoichiometry of the complex was confirmed by isolation of the most abundant charge state (+29) of its ion series in the quadrupole and subsequent collisional activation. The resulting MS^2 spectrum shows the dissociation into monomeric Pex14p and a 2:1 oligomer (*SI Appendix*, Fig. S4*A*). We further used SEC combined with multiangle light scattering (SEC-MALS) to verify the molecular mass of Pex14p(M51L)/Pex17p. The complex indeed ran at 143.9 kDa (±0.02%) consistent with the 3:1 stoichiometry (*SI Appendix*, Fig. S5*B*).

Native MS spectra of His_6-Pex14p(WT) or $Strep_{II}$-Pex14p(M51L) alone in DDM showed only the monomeric forms (*SI Appendix*, Fig. S4*B*), indicating that the coexpression of Pex17p stabilizes this complex. In contrast, SEC-MALS of Pex14p(M51L) in absence of Pex17p revealed a peak at ∼114.5 kDa, which is, however, close to the theoretical mass of 118.5 kDa for a Pex14p homotrimer (*SI Appendix*, Fig. S5*C*). We interpret these data that Pex14p homotrimers might be so unstable in absence of Pex17p that they immediately dissociate into monomers at the stage of electrospray ionization during the native MS analysis. Based on these results, we conclude that the Pex14p(M51L)/Pex17p complex consists of three copies of Pex14p(M51L) and one copy of Pex17p, with a molecular mass of ∼143 to 144 kDa.

Analysis of Pex14p(M51L)/Pex17p in DDM by negative-stain EM revealed elongated flexible pin-like particles, which however displayed limited contrast (*SI Appendix*, Fig. S3*A*). We further isolated native complexes from oleic acid-induced cells expressing Pex14p-TPA (tobacco etch virus-proteinA), as previously described (23, 37). Using Pex14p-TPA as bait, we isolated the native Pex14p/Pex17p complex from Triton X-100 solubilized whole cell membranes and analyzed again the sample by negative-stain EM (*SI Appendix*, Fig. S6 *A–D*). This analysis confirmed that the native Pex14p/Pex17p complex features the same overall architecture as the recombinantly expressed complex (*SI Appendix*, Figs. S3*A* and S6 *E* and *F*). Due to superior sample quality, further structural analyses were performed with recombinantly expressed protein complexes.

CryoEM Structure of Pex14p(M51L)/Pex17p. To optimize the sample for EM studies, we reconstituted the Pex14p(M51L)/Pex17p complex into lipid nanodiscs. Both Pex14p and Pex17p contain a single transmembrane helix, thus depending on the oligomeric state of the complex, we expect a small transmembrane domain with only few membrane-spanning helices (Fig. 1*A*). In order to prevent incorporation of multiple copies of the Pex14p/Pex17p complex within the nanodiscs, we performed the reconstitution experiments using the recently reported circular MSP1D1Δ4 to 6 nanodiscs (38) (Fig. 1*B*). The Δ4 to 6 circularized nanodisc with a diameter of 7-nm is according to our knowledge the smallest available nanodisc to date and, in addition, it shows superior stability and homogeneity in comparison to typical linear MSPs. Indeed, subsequent negative-stain EM analysis revealed high-contrast monodispersed particles, with most nanodiscs trapping only a single copy of the complex that could be easily identified and automatically picked (*SI Appendix*, Fig. S3*C*). In addition, we reconstituted Pex14p(M51L) alone (in absence of Pex17p) into the Δ4 to 6 circularized nanodisc and visualized the Pex14p complex by negative-stain EM. The respective two-dimensional (2D) class averages show particles similar to those of the Pex14p(M51L)/Pex17p complex, but the rods appear more flexible and inconsistent in length, suggesting that binding of Pex17p to Pex14p does increase the stability of the Pex14p homotrimers (*SI Appendix*, Fig. S7).

We then recorded high-contrast images of Pex14p(M51L)/Pex17p reconstituted in MSP1D1Δ4 to 6 nanodiscs using Volta phase-plate (VPP) cryoEM (Fig. 2 *A* and *B*). The digital micrographs show an even spread of elongated rod-like particles (Fig. 2 *A* and *B*), suggesting that most particles adopt a side-view orientation on the grid. Particles were selected automatically using crYOLO (39) and further processed with SPHIRE (40). Reference-free 2D class averages revealed a single copy of Pex14p(M51L)/Pex17p within the nanodisc (Fig. 2*C*). The transmembrane helices are, however, not resolved within the disk, suggesting either inaccurate alignment of the small transmembrane domain due to the compact density of the disk or flexibility of the transmembrane helices relative to the cytoplasmic rod. In contrast, the cytoplasmic domains are clearly visible, appear as five sequentially arranged globular densities, and are stiff, mostly straight, or slightly curved (Fig. 2*C*). The class averages show an average length of ∼220 Å (Fig. 2*D*) and reveal additional flexibility at the end of the rod (Movie S1). We finally computed a 10-Å three-dimensional (3D) reconstruction from ∼82,600 particles selected from the most homogeneous 2D class averages (*SI Appendix*, Fig. S8*A*). The final density map revealed a 22-nm elongated rod inserted at the periphery of the nanodisc (Fig. 2*E*). The rod appears hollow with an inner diameter of 7 Å. We further performed focused refinement of the rod after signal subtraction of the nanodisc, which improved the respective density (*SI Appendix*, Fig. S8*A*). The resulting structure can be dissembled in two structural regions, showing a kinked connection (*SI Appendix*, Fig. S8*B*).

The resolution of the structural region below the kink is now significant to allow fitting of polyalanine helices (Fig. 2*F* and Movie S2). Three long helices run approximately parallel to each other and form a 12.5-nm helical bundle (Fig. 2 *F* and *G*). The helical bundle is, however, not well ordered, showing several weak connections, suggesting thus a higher-order degree of flexibility in comparison to a typical coiled-coil structure. These weak connections do not involve, however, a change in the direction of the overall rod axis. Interestingly, two shorter α-helices complement (Fig. 2 *F* and *G*, yellow, and Movie S2) this arrangement and integrate into the helical bundle.

The overall length of 12.5-nm of each of the three long α-helices, as well as their topology directly after the membrane, agree well with the predicted coiled-coil domain 1 of Pex14p (Figs. 1*A* and 2 *F–H* and *SI Appendix*, Fig. S9). In addition, the dimensions and topology of the two shorter α-helices match the predicted coiled-coil domains 1 and 2 of Pex17p (Figs. 1*A* and 2 *F–H*).

In accordance with the native MS and SEC-MALS data suggesting a 3:1 heterotetrameric arrangement of Pex14p:Pex17p, we conclude that the lower part of the rod consists of a trimeric arrangement of the predicted coiled-coil domain 1 of Pex14p($Pex14p_{130–212}$). Three copies of this domain are directly located after the membrane and form a 12.5-nm bundle, which is in addition complemented by a single copy of Pex17p, running parallel to the rod that is thus mainly formed by Pex14p. The two shorter coiled-coil domains of Pex17p ($Pex17p_{71–89}$ and $Pex17p_{125–140}$) are tightly associated with the bundle and the rod displays at the respective segments a pseudo-fourfold symmetry (Fig. 2 *F–H*, *SI Appendix*, Fig. S8*B*, and Movie S2). The bundle is followed by a short 5.5-nm region (Fig. 2 *F* and *G* and *SI Appendix*, Fig. S8*F*), which is however kinked toward the base of the rod and less well resolved, suggesting a higher degree of structural heterogeneity and/or flexibility.

Interactions within In Vitro and Native Pex14p/Pex17p Complexes. To obtain more detailed structural information on protein interactions within the Pex14p/Pex17p complex, the complex was subjected to chemical cross-linking combined with MS analysis (XL-MS) (Fig. 3*A*). We used the cross-linker bis(sulfosuccinimidyl)suberate (BS3), which preferentially reacts with the amine group of lysine residues or protein N termini and to a lower

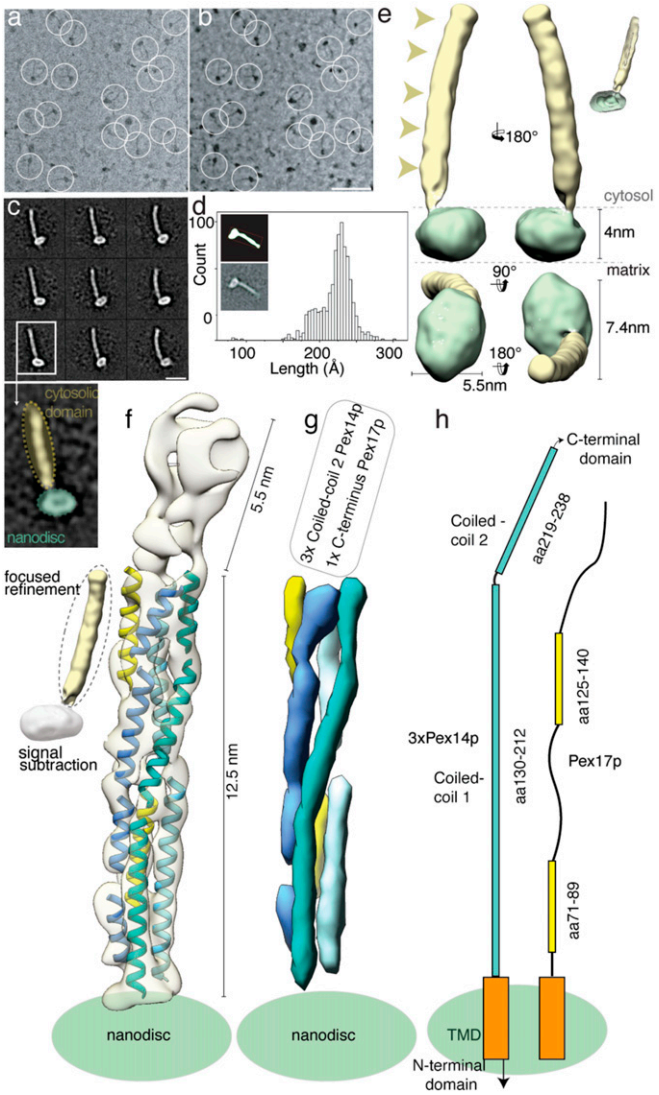

Fig. 2. CryoEM structure of the Pex14p/Pex17p complex. (*A*) Subarea of a typical low-dose VPP cryoEM micrograph of Pex14p/Pex17p reconstituted in cMSP1D1Δ4 to 6. Some particles are highlighted with white circles. (Scale bar, 50 nm.) (*B*) For better visualization we also denoised this particular micrograph using JANNI. It should be noted that denoised micrographs were not used during image processing. (*C*) Representative reference-free 2D class averages of Pex14p/Pex17p. (Scale bar, 10 nm.) The *Inset* shows one of the class averages further magnified. Densities of the nanodisc (green) and the cytosolic domains (yellow) are highlighted. (*D*) End-to-end distance of the 2D class averages. (*E*) Density map of Pex14p/Pex17p in nanodisc. Shown are different side views, after horizontal rotation of 90° around their longest axis, the bottom and top views. The rod and nanodisc density are highlighted in yellow and green, respectively. (*F*) Resulting map from focused 3D local refinement on the rod region after signal subtraction of the nanodisc. The rod region dissembled in two structural regions, showing a kinked connection. Poly-alanine helices were fitted into rod-like densities of the *Lower* rod domain of the cryoEM map and colored according to their connectivity and assignment to Pex14p (shades of blue) and Pex17p (yellow). (*G*) For better visualization and comparison, a density map was simulated from the polyalanine helices at a resolution of 8.5 Å. Fitting of α-helices was not possible in the *Upper* rod domain (white box), due to limited resolution. Note that the moderate resolution of the cryoEM structure does not allow registration of the amino acid positions. (*H*) Schematic of the topology of the predicted coiled-coil domains of yeast Pex14p and Pex17p compared to the cryoEM structure (transmembrane domains: orange; coiled-coil domains Pex14p: cyan; coiled-coil domains Pex17p: yellow). The N- and C-terminal domains of Pex14p are not shown.

extent with the hydroxy-group of serine, threonine, or tyrosine residues spanning a maximum distance of 11.4 Å (41). Pex14p and Pex17p display intermolecular linkages (red lines, Fig. 3*A*) along the complete sequence of Pex17p. Pex14p/Pex14p homomultimeric linkages (blue lines, Fig. 3*A*) span the same range being localized within and close to the N-terminal three-helix domain of Pex14p as well as along its predicted coiled coils.

These data are in agreement with the cryoEM structure and ab initio structure predictions of Pex14p and Pex17p (Fig. 3*B*), indicating not only a parallel arrangement between adjacent predicted coiled-coil domains of Pex14p, but also a parallel arrangement and interactions between adjacent predicted coiled-coil domains of Pex14p and Pex17p molecules, thereby forming the helical extramembrane coiled-coil-like rod.

The ab initio structure predictions suggest a ∼7-nm helical arrangement at the C-terminal end of Pex17p (Fig. 3*B*). Furthermore, XL-MS linkages indicate major contacts from residues Lys177 and Lys189 of the C-terminal end of Pex17p to residues Ser214, Lys227, and Lys233 of the second predicted coiled coil of Pex14p (Fig. 3 *A* and *B*). The direct comparison of the structure predictions with the cryoEM density under consideration of XL-MS linkages (Fig. 3*B*) suggests that the 5.5-nm rod-like domain above the kink, that is not as well resolved in our cryoEM structure (Fig. 2 *F* and *G*), most likely contains three copies of coiled-coil domain 2 of Pex14p and the C-terminal end of Pex17p (Fig. 3*B*).

Furthermore, these linkages are in agreement with previous results identifying the extreme C terminus of Pex17p (corresponding to amino acids [aa] 167 to 199) as the smallest fragment that is sufficient for Pex14p-interaction (42). Additional interfaces were identified between the N-terminal domains of Pex14p (Lys52, Lys67) and Pex17p (Lys20-21, Thr28), indicating further secondary contacts between both proteins (Fig. 3*B*).

Gray lines in Fig. 3*A* represent intra- or intermolecular contacts and most of them span the N-terminal domain of Pex14p. These contacts are in agreement with the previous crystal structure of the conserved N-terminal domain of Pex14p displaying a three-helix bundle (43) and possibly include further intermolecular connections between adjacent Pex14p molecules. A few additional connections span the TMD of Pex14p and Pex17p (gray lines, Fig. 3*A*). Note, however, that lysine 67 located between the N-terminal domain and the TMD of Pex14p displays the highest number of connections reaching all three N-terminal helices, the same linker region of adjacent Pex14p as well as the N-terminal part of Pex17p. This supports the presence of a highly flexible linker and may explain sporadic contacts around the detergent micelle to the C-terminal side of the TMD. Furthermore, the observed connections within the Pex14p/Pex17p complex are generally very similar to those reported for Triton X-100 solubilized complexes of Pex14p, Pex17p, and Dyn2p (24).

To further characterize the Pex14p/Pex17p interactions, we performed domain-mapping experiments based on the yeast two-hybrid system with $Pex17p_{167–199}$ fused to the Gal4p–DNA binding domain (DB) and Gal4p–DNA-activation domain fusions of progressive carboxyl- and/or amino-terminal truncations of Pex14p. In line with previous findings, coexpression of $Pex17p_{167–199}$ with full-length Pex14p resulted in considerable β-galactosidase, demonstrating the interaction of both proteins (42) (Fig. 3*C*). However, Pex14p lacking N- or C-terminal regions did still interact with $Pex17p_{167–199}$, pointing to an internal binding region. In fact, we identified the second putative coiled-coil domain plus a part of the first coiled-coil domain of Pex14p and a C-terminal portion as sufficient to mediate interaction to $Pex17p_{167–199}$ (Fig. 3*C*). This is in line with the XL-MS data, which also revealed the second putative coiled-coil domain of Pex14p as a major interaction site with Pex17p (red lines, Fig. 3 *A* and *B*).

Of note, Pex17p lacking its C terminus did not interact with Pex14p in yeast two-hybrid assays (42), although further N-terminal contacts were detected by XL-MS (Fig. 3*A*). Thus, in

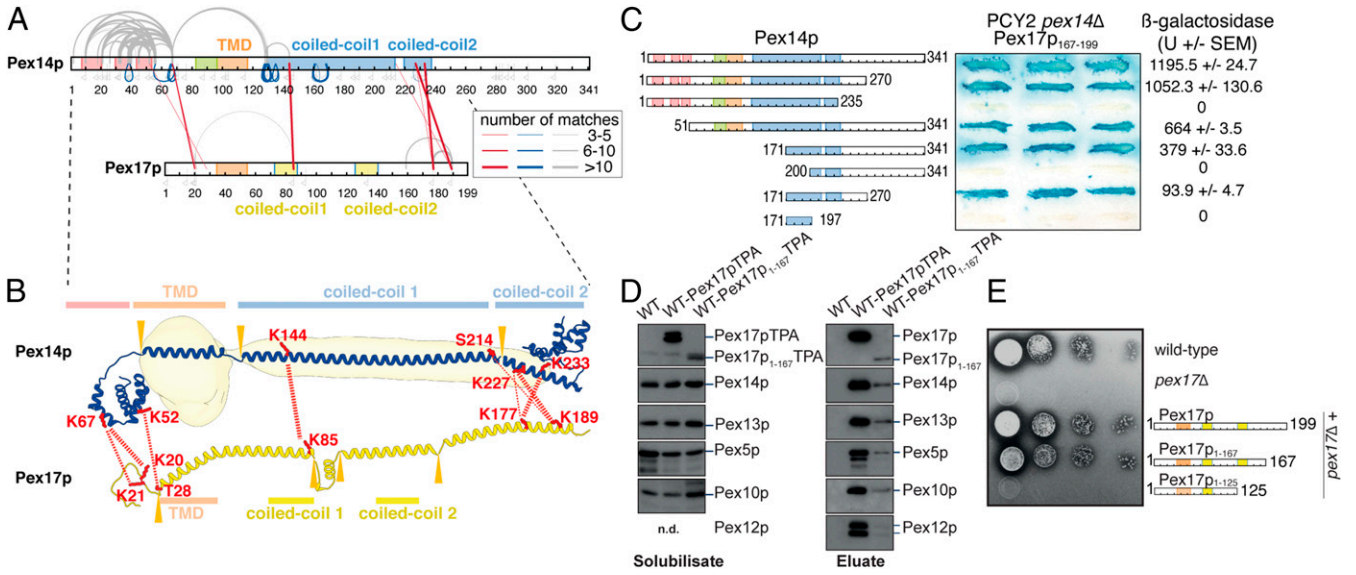

Fig. 3. Characterization of the interactions between Pex14p and Pex17p. (*A*) Map of connections between side chains of Pex14p and Pex17p identified by XL-MS. Purified $Strep_{II}$-Pex14p/His_6-Pex17p complexes were cross-linked using BS3 and subjected to in-solution digestion using trypsin. Straight red lines represent intermolecular cross-links, gray curved lines intra- or intermolecular cross-links, and blue lines indicate homomultimeric linkages. The line thicknesses indicate the number of matches found for each cross-link. Gray flags denote identifications of residues modified by the hydrolyzed cross-linker. All cross-link identifications can be found in Dataset S1. (*B*) Structure prediction of Pex14p and Pex17p overlaid with our cryoEM density of the Pex14p/Pex17p complex. An ab initio 3D structure prediction of the individual proteins using trRosetta (57) was manually expanded to visualize the secondary structure elements of the prediction and their potential position in our cryoEM density. The positions at which the model of the prediction was manually rearranged are indicated by orange triangles, and the predicted secondary structure elements are indicated. The amino acid residues that form intermolecular cross-links between Pex14p and Pex17p in our cross-linking experiment are marked as red sticks, and the observed cross-linking pattern as red dashed lines. (*C*) Gal4p binding domain (DB)/Pex14p fusions with progressive N- and/or C-terminal deletions of Pex14p were assayed for their interaction with $Pex17p_{167–199}$. Double transformants of PCY2 *pex14*Δ cells expressing the indicated fusion proteins were selected, and β-galactosidase activity was determined by a filter assay using X-gal as substrate. Three representative independent double transformants are shown. The β-galactosidase activity shown on the *Right* is the average of triplicate measurements for three independent transformants harboring each set of plasmids. SEM, SE of mean; U, units. (*D*) Native complexes were isolated from solubilized membrane fractions from wild-type cells expressing either Pex17pTPA or $Pex17p_{1–167}$TPA eluted from IgG-Sepharose with TEV protease. An eluate of wild-type cells served as control. Equal portion of the solubilisate (*Left*) and eluate (*Right*) were subjected to immunoblot analysis with antibodies as indicated. (*E*) Cells of wild-type, *pex17*Δ, or *pex17*Δ cells expressing plasmid-based Pex17p variants as indicated were grown overnight on glucose minimal media. Subsequently,10-fold dilutions were prepared, and 2 μL of each dilution were spotted onto oleate plates, which were scored for the appearance of colonies and halo formation. In contrast to wild-type cells, *pex17*Δ mutant was not able to utilize oleate. Expression of wild-type Pex17p as well as $Pex17p_{1–167}$ restored the growth defect of *pex17*Δ cells, whereas $Pex17p_{1–125}$ lost its ability for functional complementation.

order to characterize possible secondary binding sites, Pex17p lacking its C terminus ($Pex17p_{1–167}$) was analyzed in its endogenous environment, the peroxisomal membrane, instead of the nucleus, as is the case in yeast two-hybrid assays. To this end, a wild-type strain expressing either Pex17p or $Pex17p_{1–167}$ genomically tagged with protein A (Pex17pTPA, $Pex17p_{1–167}$TPA) with a TEV cleavage site between both fusion partners was used. In line with published data and the function of Pex17p as a constituent of the receptor docking complex, Pex13p, Pex14p as well as the PTS1-receptor Pex5p, were coisolated when full-length Pex17p served as bait (Fig. 3*D*) (44). As originally described (23), other components of the importomer, represented by the two RING-finger proteins Pex10p and Pex12p, were also part of the Pex17p complex. Pex17p lacking its C-terminal Pex14p binding module displayed a significant reduction in its steady-state level when compared with wild-type protein and the constituents of the importomer that were present in the Pex17p complex, were also associated with $Pex17p_{1–167}$TPA, albeit in a much lower amount (Fig. 3*D*). Thus, the results demonstrate that $Pex17p_{1–167}$ is still associated with the importomer, although it is lacking its C-terminal Pex14p binding region. This is again in line with the XL-MS results, corroborating that interactions between the first putative coiled coils and between the N termini of coexpressed Pex14p and Pex17p (Fig. 3 *A* and *B*) promote the insertion of $Pex17p_{1–167}$ into Pex14p membrane complexes (Fig. 3*D*). Interestingly, growth on oleic acid of cells deficient in Pex17p was restored upon expression of $Pex17p_{1–167}$, indicating that the truncated $Pex17p_{1–167}$ is biologically active (Fig. 3*E*).

Intermolecular Interactions within the Predicted Coiled-Coil Domains of Pex14p Are Essential for Its Oligomerization. To assess which of the Pex14p/Pex14p interactions are essential for oligomerization, we used recombinantly expressed truncated Pex14p variants and monitored formation of oligomers by chemical cross-linking and native MS. One N-terminal variant, $Pex14p_{1–95}$, and two C-terminal variants comprising solely the second coiled-coil domain ($Pex14p_{213–341}$) or both coiled-coil domains ($Pex14p_{119–341}$), were incubated with the cross-linker BS3 and products of the reactions separated by SDS/PAGE (sodium dodecyl sulfate polyacrylamide gel electrophoresis) (Fig. 4*A*). Whereas the N-terminal and the shorter C-terminal variant remained in the monomeric form, the larger C-terminal variant including both coiled-coil domains showed additional bands indicative of the formation of dimers and trimers (Fig. 4*A*). With increasing concentrations of the cross-linker, the trimer band became stronger than the dimer band, but no higher molecular weight bands of tetrameric or higher oligomeric species appeared (*SI Appendix*, Fig. S10). The same Pex14p variants were analyzed by native MS to study their oligomerization behavior (Fig. 4*B*). In line with the cross-linking results, the two shorter variants were observed solely monomeric, whereas the longer variant comprising both coiled-coil domains predominantly formed trimers and, to a considerably lesser extent, dimers and monomers.

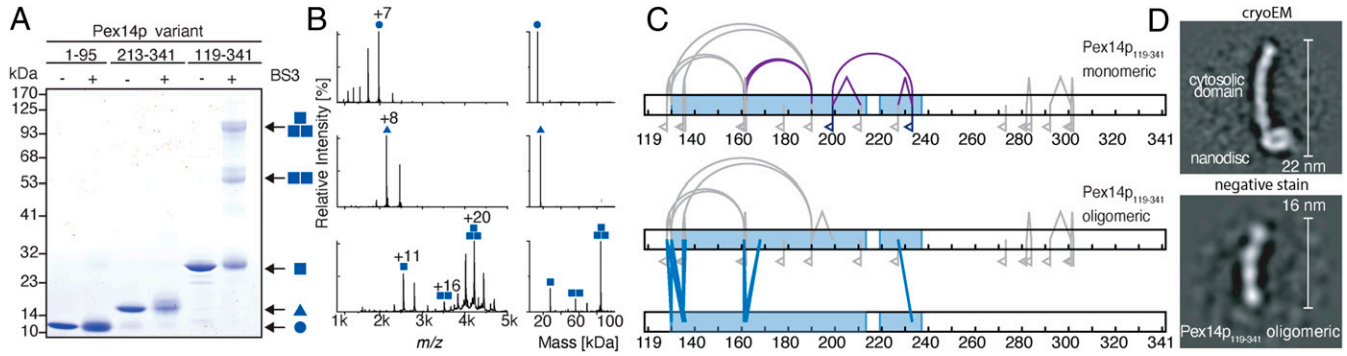

Fig. 4. Oligomerization properties of Pex14p variants. (*A*) Recombinant variants of Pex14p comprising its N-terminal domain (Pex14p$_{1–95}$; calculated molecular mass of 13.8 kDa; circle), a shorter (Pex14p$_{213–341}$; 17.3 kDa; triangle) and a longer C-terminal part (Pex14p$_{119–341}$; 28.1 kDa; square) were cross-linked using BS3 and separated by SDS/PAGE. Bands assigned to monomeric, dimeric, and trimeric forms are marked by one, two, or three symbols. (*B*) Native MS of Pex14p$_{1–95}$ (*Top*), Pex14p$_{213–341}$ (*Middle*), and Pex14p$_{119–341}$ (*Bottom*). Main charge states are indicated based on assignments of peak series to monomeric and oligomeric complexes. The respective charge-state deconvoluted spectra are shown on the *Right* and indicate molecular masses of the monomeric proteins (*Top*: observed molecular mass of 13.8 kDa; *Middle*: 17.3 kDa; and *Bottom*: 28.1 kDa) as well as the dimeric and trimeric Pex14p$_{119–341}$ (*Bottom*: 56.2 kDa and 84.3 kDa). (*C*) Schematic view of homomultimeric (straight blue lines) and intramolecular (gray curved lines) cross-links as well as peptide modifications by loop links (gray angled lines) and monolinks (flags) identified and quantified by LC-MS in monomeric (*Top*) and trimeric (*Bottom*) Pex14p$_{119–341}$. Quantitative analysis further distinguished linkages recovered equally from monomeric and trimeric forms (gray) and monomer-specific linkages (purple). All quantified cross-link residue pairs can be found in Dataset S2. (*D*) Side-by-side comparison between reference-free class averages of Strep$_{II}$-Pex14p(M51L)/His$_6$-Pex17p in nanodisc (cryoEM) and the homotrimeric Pex14p$_{119–341}$ variant (negative stain).

From the cross-linking experiment, gel-separated monomeric and oligomeric forms of Pex14p$_{119–341}$ were subjected to digestion using trypsin and liquid chromatography-tandem mass spectrometry (LC-MS/MS) for peptide identification. In addition, a quantitative MS analysis was performed, enabling a direct comparison of the abundance of individual cross-linked peptides identified in the trimer to those in the monomer (*SI Appendix*, Fig. S11). The map of interactions resulting from this analysis is summarized in Fig. 4*C*. We identified a set of 13 residue pairs specifically enriched with the trimer representing (homomultimeric) intermolecular interactions along the full region of both predicted coiled-coil domains (Fig. 4*C*, blue lines, and *SI Appendix*, Fig. S11*C*, red dots). Four cross-linked residue pairs, Lys128 and Lys130 to Lys161 as well as Lys130 and Lys135 to Lys190 had ratios close to 1:1 and thus were present in almost equal abundance in monomers and oligomers (Fig. 4*C*, gray lines, and *SI Appendix*, Fig. S11*C*, red dots). They represent contacts between the beginning and the center of Pex14p's coiled-coil domain 1 (Fig. 4*C*, gray lines) and were not identified in the Pex14p/Pex17p complex (see Fig. 3*A*), indicating a higher degree of flexibility of this part of Pex14p in the absence of its TMD and Pex17p. Of note, one residue pair of high abundance (199/233) and two pairs of lower abundance (162/190 and 161/190) were monomer specific (Fig. 4*C*, purple lines, and *SI Appendix*, Fig. S11*C*), suggesting that these linkages may prevent assembly into oligomeric forms. This is in agreement with their absence in the pattern of connections detected in the Pex14p/Pex17p complex (compare Fig. 3*A*).

In conclusion, in vitro formation of Pex14p oligomers (predominantly homotrimers) required the presence of its first coiled-coil domain. The identified intermolecular interactions along the full length of both predicted coiled-coil domains of Pex14p homotrimers confirm the parallel assembly of the individual molecules. Connections between the two coiled-coil domains within Pex14p monomers in absence of the transmembrane domain interfere with the formation of higher oligomers, possibly by forcing bended conformations not compatible with the parallel geometry.

We further subjected the longer trimeric variant (Pex14p$_{119–341}$ homotrimers including the two coiled-coil domains and the C-terminal domain of Pex14p) to negative-stain analysis. The trimeric subcomplex forms 16-nm rods that appear similar to the full-length Pex14p/Pex17p complex without the nanodisc density (Fig. 4*D* and *SI Appendix*, Fig. S12). This further confirms that three parallel arranged predicted coiled-coil domains of Pex14p indeed assemble to form the backbone of the elongated extramembrane rod-like domain of the Pex14p/Pex17p complex.

Membrane Topology of Pex14p/Pex17p. At this point, it is important to emphasize that yeast Pex14p contains two binding sites for the PTS1 receptor Pex5p: the first at the N-terminal domain and the second at the C-terminal domain (Fig. 1*A*). Both domains are not resolved in our cryoEM structure. The C-terminal domain of Pex14p (~100 aa) is predicted to be intrinsically disordered and thus highly flexible, whereas the N-terminal domain is highly conserved and forms a three-helix bundle (43), which is however connected to the transmembrane domain by a long flexible linker peptide (*SI Appendix*, Fig. S9), allowing apparently a high degree of flexibility. With regard to Pex17p, only the helices forming the two-short coiled-coil domains above the membrane are identified in our cryoEM structure.

To verify the presence of the N-terminal domains of both Pex14p and Pex17p within the rod complexes observed by cryoEM and clarify their membrane topology, we coexpressed (Pex14p/His$_6$-Pex17p) and (His$_6$-Pex14p/Pex17p), reconstituted the respective complex in MSP1D1ΔH5 nanodiscs, labeled with Ni-NTA gold, and imaged by negative-stain EM (Fig. 5 *A* and *B* and *SI Appendix*, Fig. S13). In both cases, the gold particles bound below the nanodiscs, suggesting colocalization of the N termini of Pex14p and Pex17p. This is in agreement with the XL-MS data that revealed linkages between the N-terminal domains of Pex14p (Lys67) and Pex17p (Lys20 and Lys21) (Fig. 3 *A* and *B*).

In order to exclude the possibility that the narrow nanodiscs prevent the formation of higher-order assemblies and challenge the oligomerization and overall structure of the Pex14p/Pex17p complex in a more close-to-native lipid environment and membrane curvature, we reconstituted the complex in liposomes and visualized the liposomes by negative-stain EM and cryoET (Fig. 5 *C–E*). After successful reconstitution, the liposomes were shaped like sea urchins, with multiple copies of rods (spikes) covering isotropically their outer surface. The 20-nm single rods were visible around the circumference of the liposomes mostly arranged perpendicular to the bilayer plane, clearly resembling

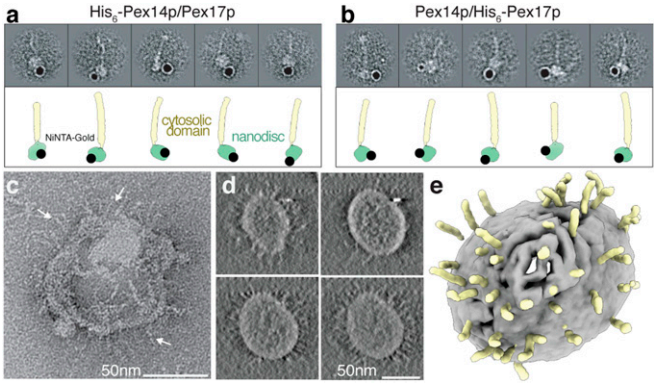

Fig. 5. Immunogold labeling of the N termini of Pex14p/Pex17p and incorporation into liposomes. (*A*, *B*) Localization of the N-terminal His_6-tag in the recombinant His_6-Pex14p(M51L)/Pex17p (*A*) and Pex14p(M51L)/His_6-Pex17p (*B*) with Ni-NTA nanogold. The topology of the gold label is also shown graphically mapped on the model of Pex14p/Pex17p. The N termini of both proteins are clearly located closely to the nanodisc MSP1D1ΔH5. (*C*) Representative negative-stain image of Pex14p/Pex17p incorporated into liposomes. (*D* and *E*) Slices through the tomographic cryoEM volume of a single Pex14p/Pex17p liposome (*D*) and corresponding 3D segmentation (*E*), showing the bilayer (gray) and the characteristic Pex14p/Pex17p rods (yellow).

the cryoEM structure in the nanodisc (Fig. 5 *C–E* and Movie S3). Pex14p/Pex17p do not form larger supercomplexes upon liposome incorporation.

Discussion

It is well established that Pex13p, Pex14p, and Pex17p mediate the docking of cytosolic receptor–cargo complexes to the peroxisomal membrane (10–14, 45–47). Pex13p and Pex14p recognize and physically bind both of the import receptors, Pex5p and Pex7p. This, and the fact that Pex17p interacts with Pex14p (14, 47, reviewed in ref. 48) led to the conclusion that these three peroxins form the receptor–docking complex. However, docking of the receptor cargo complex supposedly is mediated by Pex14p (21, 22). Along this line, transport of the peroxin Pex8p into peroxisomes, requires only the presence of Pex14p and the import receptor Pex5p (49). Moreover, in vitro, Pex5p and Pex14p alone are capable of forming a gated ion-conducting channel (15). Taken together, these data suggest that Pex14p oligomers constitute minimal receptor–docking complexes.

In our study, we characterize the overall architecture of Pex14p in complex with Pex17p. We show that Pex14p and Pex17p together form a ∼143-kDa rod-like complex (Fig. 1*C* and *SI Appendix*, Fig. S5), containing three copies of Pex14p and one copy of Pex17p. The cryoEM structure suggests a homotrimeric parallel helical bundle formed by three copies of the predicted coiled-coil domain 1 of Pex14p and further association of both predicted coiled-coil domains of a single Pex17p copy into this arrangement (Fig. 6*A*). The resulting heterotetrameric parallel α-helical bundle shows however several kinks and does not display a typical tetrameric coiled-coil structure, as we initially expected, thereby allowing possibly a higher degree of flexibility. The XL-MS data, the yeast two-hybrid assays, and functional expression of a Pex17p variant suggest a parallel arrangement of Pex14p and Pex17p along their complete sequence (Fig. 6*A*). Importantly, we show that both predicted coiled-coil domains of Pex14p are required for its homooligomerization (Fig. 4).

Pex17p has been identified in yeast, whereas a human counterpart is missing. According to previous studies, Pex17p seems dispensable for receptor docking, but important to increase the efficiency of the docking event (23, 24). Our data suggest that in absence of Pex17p yeast Pex14p is capable of forming rod-like homotrimers (*SI Appendix*, Fig. S5*C*), which are however more heterogeneous and flexible compared to the Pex14p/Pex17p complex (*SI Appendix*, Fig. S7). Pex17p associates tightly with Pex14p and increases the stability of the Pex14p homotrimers. Thus, Pex17p might not be required for peroxisomal protein translocation or pore formation per se but for the stabilization of higher oligomeric state Pex14p complexes. Such a supporting function seems not to be required in higher eukaryotes. Indeed, mammalian Pex14p does not contain the predicted coiled-coil domain 2, which according to our data is one of the main interaction sites to Pex17p in yeast, and might thus possess altered oligomer stability and/or oligomerization properties in general (50).

The topology of Pex14p at the peroxisomal membrane has been a matter of debate. However, it is well established in the field, that the C-terminal two-thirds of Pex14p are exposed into the cytosol (46, 51). The EM analysis clearly shows these structural regions, including the predicted coiled-coil domains, located above the nanodisc. The C-terminal domain of Pex14p (∼100 aa) is not resolved in our cryoEM structure. According to secondary and 3D structure predictions (Fig. 3*B* and *SI Appendix*, Fig. S9*A*), this domain containing the cytosolic receptor binding domain is apparently flexible. Furthermore, the three C-terminal domains of Pex14p within the Pex14p/Pex17p complex do not show homomultimeric linkages (Fig. 3*A*), suggesting that they do not homooligomerize but possibly flexibly wobble around the helical rod instead (Fig. 6*A*). Gold-labeling experiments allowed us to directly detect the N termini of both Pex14p and Pex17p colocalized below the nanodisc, hence on the opposite side of the membrane with regard to the cytosolic C-terminal domains. According to our results, the two receptor binding sites of Pex14p are thus located on opposite sides of the peroxisomal membrane: the first at the N-terminal domain (intraperoxisomal) and the second at the C-terminal domain (facing the cytosol) (52). In addition, the 2D class averages of Pex14p/Pex17p indicate that the conserved N-terminal domain is highly flexible, only appearing as blurry density below the nanodisc (Movie S1).

The N-terminal domain of Pex14p, which also contains one of the receptor binding sites, is indeed connected to the transmembrane domain by a flexible interdomain linker peptide (*SI Appendix*, Fig. S9 and Fig. 6*A*).

The cryoEM tomograms of reconstituted Pex14p/Pex17p in liposomes revealed isotropic decoration of the liposomes by the complex resulting in a sea urchin-like proteoliposome. Thus, the Pex14p/Pex17p complexes do not locally modify membrane curvature and do not form higher-order assembly structures or clusters in the close-to-native lipid environment of a liposome.

Our data thus strongly indicate that the peroxisomal docking complex, mainly formed by Pex14p, resembles a rod-like structure that emanates into the cytosol and uses highly flexible terminal peptides to recruit the cargo-loaded receptor complexes (Fig. 6*B*). The further steps of pore formation and cargo translocation can only be speculated at this stage. The overall Pex14p architecture presented in this study renders the possibility of entry of further Pex14p domains into the membrane upon receptor binding rather unlikely. A cluster of charged residues in-between the transmembrane helix and the first coiled-coil helix (*SI Appendix*, Fig. S9) would prevent insertion of the coiled-coil helices into the membrane bilayer. The possible distance of the C-terminal receptor binding site to the membrane is unlikely to allow entry of this unstructured domain into the membrane without dramatic conformational changes of the predicted coiled-coil domain. Furthermore, the α-helices of the conserved intraperoxisomal N-terminal domain containing the first receptor binding site are not amphipathic, and thus not capable of entering the membrane (Fig. 6*B*). The overall fishing rod-like architecture of the complex suggests a pivotal role of Pex14p in recruitment of Pex5p/cargo complexes. The rod-like domains position the flexible C-terminal tail of Pex14p far into the

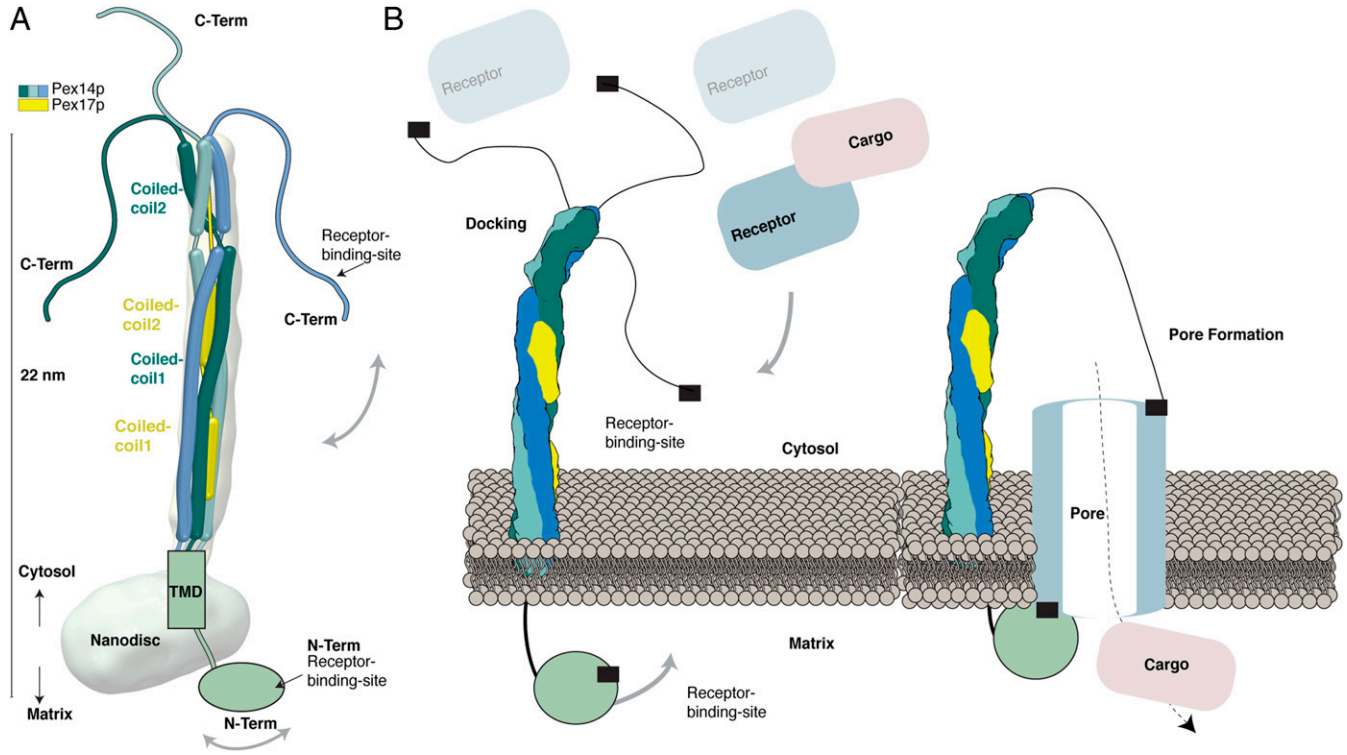

Fig. 6. Organization of the Pex14p/Pex17p complex. (*A*) Model of the Pex14p/Pex17p complex. The topology and arrangement of the different domains are indicated, according to the results of the present study. (*B*) Model for triggering peroxisomal translocation upon binding of the receptor–cargo complex to Pex14p/Pex17p at the peroxisomal membrane.

cytosol. This way, a maximal amount of cargo–receptor complexes in the vicinity of the peroxisome can be captured and fixed in proximity to the peroxisomal membrane to enforce the formation of the translocation pore. This would imply that the pore may be exclusively formed by the receptor Pex5p, which is in line with the transient pore model (53), suggesting that Pex5p is functioning like a pore-forming toxin (Fig. 6*B*). Indeed, import-deficient *pex14Δ* yeast mutants are capable of importing matrix proteins after Pex5p overexpression (54) and in vitro, Pex5p is capable of entering the membrane without any help from the docking complex, when present at high concentrations (55). The interaction of the N-terminal domain of Pex14p to membrane-embedded Pex5p might then further stabilize the Pex5p transient pore assembly (Fig. 6*B*).

Our results provide mechanistic insight into the yeast peroxisomal docking complex and thus into major aspects of the peroxisomal import machinery in general. Achieving near atomic resolution is beyond our grasp now, but we are confident that our study will provide a strong foundation and trigger future in vivo and in vitro structural and integrative studies of higher-order assemblies, toward understanding key events of peroxisomal translocation.

Materials and Methods

Strains (*SI Appendix*, Table S1), culture conditions, plasmids (*SI Appendix*, Table S2), yeast cell extraction including two-hybrid analysis and isolation of the native Pex14p/Pex17p complex, were performed in this study and are provided in *SI Appendix*. Protein purification and corresponding immunoblotting including antibodies as well as SEC-MALS were performed as described and listed in *SI Appendix*, *SI Materials and Methods*. Details for negative-stain electron microscopy, cryoEM, sample preparation including reconstitution studies and processing strategy in SPHIRE, are provided in *SI Appendix*. Native MS and LC-MS including the associated proteolytic digestion and chemical cross-linking are described in *SI Appendix*.

Data Availability. The EM density map has been deposited in the Electron Microscopy Data Bank under accession code EMD-12047. MS raw data and result files have been deposited in the ProteomeXchange Consortium via the PRIDE repository (56) and are publicly accessible from its website with the dataset identifier PXD016304. All study data are included in the article and supporting information.

ACKNOWLEDGMENTS. We are grateful to D. Prumbaum for excellent assistance with electron microscope facilities and S. Tacke for acquisition of the tomographic tilt series. We thank Raphael Gasper-Schoenenbruecher for his excellent support during SEC-MALS data collection and analysis, as well as fruitful discussions. We also thank Thomas Schröter and Sven Fischer for experiments during the initial phase of this work; Bettina Knapp for technical assistance with LC/MS analyses; as well as Carol Robinson, Carla Schmidt, and Jan Commandeur (MS Vision) for support and discussions on native MS. C.G. thanks Stefan Raunser for continuous support and I. Vetter for stimulating discussions. This work was supported by the Max Planck Society, the Deutsche Forschungsgemeinschaft (DFG, German Research Foundation) (FOR1905 to C.G., R.E., and B.W.). Work in the B.W. laboratory was also funded by the DFG, Project-ID 278002225, RTG 2202, and Project-ID 403222702, SFB 1381; the Excellence Strategy (CIBSS, EXC-2189, Project-ID 390939984); and the Excellence Initiative of the German federal and state governments (EXC 294, BIOSS). Work included in this study has also been performed in partial fulfillment of the doctoral theses of P.L., T.H., and D.W.

1. N. E. Braverman *et al.*, Peroxisome biogenesis disorders in the Zellweger spectrum: An overview of current diagnosis, clinical manifestations, and treatment guidelines. *Mol. Genet. Metab.* **117**, 313–321 (2016).
2. H. R. Waterham, S. Ferdinandusse, R. J. A. Wanders, Human disorders of peroxisome metabolism and biogenesis. *Biochim. Biophys. Acta* **1863**, 922–933 (2016).
3. P. B. Lazarow, Y. Fujiki, Biogenesis of peroxisomes. *Annu. Rev. Cell Biol.* **1**, 489–530 (1985).
4. J. R. Glover, D. W. Andrews, R. A. Rachubinski, Saccharomyces cerevisiae peroxisomal thiolase is imported as a dimer. *Proc. Natl. Acad. Sci. U.S.A.* **91**, 10541–10545 (1994).
5. J. A. McNew, J. M. Goodman, An oligomeric protein is imported into peroxisomes in vivo. *J. Cell Biol.* **127**, 1245–1257 (1994).
6. S. Hasan, H. W. Platta, R. Erdmann, Import of proteins into the peroxisomal matrix. *Front. Physiol.* **4**, 261 (2013).

7. P. E. Purdue, P. B. Lazarow, Peroxisome biogenesis. *Annu. Rev. Cell Dev. Biol.* **17**, 701–752 (2001).
8. L.-A. Brown, A. Baker, Peroxisome biogenesis and the role of protein import. *J. Cell. Mol. Med.* **7**, 388–400 (2003).
9. W. Girzalsky, D. Saffian, R. Erdmann, Peroxisomal protein translocation. *Biochim. Biophys. Acta* **1803**, 724–731 (2010).
10. M. Albertini *et al*., Pex14p, a peroxisomal membrane protein binding both receptors of the two PTS-dependent import pathways. *Cell* **89**, 83–92 (1997).
11. Y. Elgersma *et al*., Analysis of the carboxyl-terminal peroxisomal targeting signal 1 in a homologous context in Saccharomyces cerevisiae. *J. Biol. Chem.* **271**, 26375–26382 (1996).
12. R. Erdmann, G. Blobel, Identification of Pex13p a peroxisomal membrane receptor for the PTS1 recognition factor. *J. Cell Biol.* **135**, 111–121 (1996).
13. S. J. Gould *et al*., Pex13p is an SH3 protein of the peroxisome membrane and a docking factor for the predominantly cytoplasmic PTs1 receptor. *J. Cell Biol.* **135**, 85–95 (1996).
14. B. Huhse *et al*., Pex17p of Saccharomyces cerevisiae is a novel peroxin and component of the peroxisomal protein translocation machinery. *J. Cell Biol.* **140**, 49–60 (1998).
15. M. Meinecke *et al*., The peroxisomal importomer constitutes a large and highly dynamic pore. *Nat. Cell Biol.* **12**, 273–277 (2010).
16. M. Meinecke, P. Bartsch, R. Wagner, Peroxisomal protein import pores. *Biochim. Biophys. Acta* **1863**, 821–827 (2016).
17. M. Montilla-Martinez *et al*., Distinct pores for peroxisomal import of PTS1 and PTS2 proteins. *Cell Rep.* **13**, 2126–2134 (2015).
18. N. Miyata, Y. Fujiki, Shuttling mechanism of peroxisome targeting signal type 1 receptor Pex5: ATP-independent import and ATP-dependent export. *Mol. Cell. Biol.* **25**, 10822–10832 (2005).
19. H. W. Platta, S. Grunau, K. Rosenkranz, W. Girzalsky, R. Erdmann, Functional role of the AAA peroxins in dislocation of the cycling PTS1 receptor back to the cytosol. *Nat. Cell Biol.* **7**, 817–822 (2005).
20. W. Schliebs, W. Girzalsky, R. Erdmann, Peroxisomal protein import and ERAD: Variations on a common theme. *Nat. Rev. Mol. Cell Biol.* **11**, 885–890 (2010).
21. H. Otera *et al*., The mammalian peroxin Pex5pL, the longer isoform of the mobile peroxisome targeting signal (PTS) type 1 transporter, translocates the Pex7p.PTS2 protein complex into peroxisomes via its initial docking site, Pex14p. *J. Biol. Chem.* **275**, 21703–21714 (2000).
22. A. J. Urquhart, D. Kennedy, S. J. Gould, D. I. Crane, Interaction of Pex5p, the type 1 peroxisome targeting signal receptor, with the peroxisomal membrane proteins Pex14p and Pex13p. *J. Biol. Chem.* **275**, 4127–4136 (2000).
23. B. Agne *et al*., Pex8p: An intraperoxisomal organizer of the peroxisomal import machinery. *Mol. Cell* **11**, 635–646 (2003).
24. A. Chan *et al*., Pex17p-dependent assembly of Pex14p/Dyn2p-subcomplexes of the peroxisomal protein import machinery. *Eur. J. Cell Biol.* **95**, 585–597 (2016).
25. A. Schell-Steven *et al*., Identification of a novel, intraperoxisomal pex14-binding site in pex13: Association of pex13 with the docking complex is essential for peroxisomal matrix protein import. *Mol. Cell. Biol.* **25**, 3007–3018 (2005).
26. W. Girzalsky *et al*., Involvement of Pex13p in Pex14p localization and peroxisomal targeting signal 2-dependent protein import into peroxisomes. *J. Cell Biol.* **144**, 1151–1162 (1999).
27. K. Niederhoff *et al*., Yeast Pex14p possesses two functionally distinct Pex5p and one Pex7p binding sites. *J. Biol. Chem.* **280**, 35571–35578 (2005).
28. R. Itoh, Y. Fujiki, Functional domains and dynamic assembly of the peroxin Pex14p, the entry site of matrix proteins. *J. Biol. Chem.* **281**, 10196–10205 (2006).
29. J. E. Azevedo, W. Schliebs, Pex14p, more than just a docking protein. *Biochim. Biophys. Acta* **1763**, 1574–1584 (2006).
30. W. Schliebs *et al*., Recombinant human peroxisomal targeting signal receptor PEX5. Structural basis for interaction of PEX5 with PEX14. *J. Biol. Chem.* **274**, 5666–5673 (1999).
31. J. Saidowsky *et al*., The di-aromatic pentapeptide repeats of the human peroxisome import receptor PEX5 are separate high affinity binding sites for the peroxisomal membrane protein PEX14. *J. Biol. Chem.* **276**, 34524–34529 (2001).
32. H. Otera *et al*., Peroxisomal targeting signal receptor Pex5p interacts with cargoes and import machinery components in a spatiotemporally differentiated manner: Conserved Pex5p WXXXF/Y motifs are critical for matrix protein import. *Mol. Cell. Biol.* **22**, 1639–1655 (2002).
33. A. Neuhaus *et al*., A novel Pex14 protein-interacting site of human Pex5 is critical for matrix protein import into peroxisomes. *J. Biol. Chem.* **289**, 437–448 (2014).
34. A. Barros-Barbosa *et al*., Membrane topologies of PEX13 and PEX14 provide new insights on the mechanism of protein import into peroxisomes. *FEBS J.* **286**, 205–222 (2019).
35. L. Li *et al*., Pex14/17, a filamentous fungus-specific peroxin, is required for the import of peroxisomal matrix proteins and full virulence of Magnaporthe oryzae. *Mol. Plant Pathol.* **18**, 1238–1252 (2017).
36. A. Laganowsky, E. Reading, J. T. S. Hopper, C. V. Robinson, Mass spectrometry of intact membrane protein complexes. *Nat. Protoc.* **8**, 639–651 (2013).
37. T. Hansen *et al*., Isolation of native soluble and membrane-bound protein complexes from yeast Saccharomyces cerevisiae. *Methods Mol. Biol.* **1595**, 37–44 (2017).
38. J. Miehling, D. Goricanec, F. Hagn, A split-intein-based method for the efficient production of circularized nanodiscs for structural studies of membrane proteins. *ChemBioChem* **19**, 1927–1933 (2018).
39. T. Wagner *et al*, SPHIRE-crYOLO is a fast and accurate fully automated particle picker for cryo-EM. *Commun. Biol.* **2**, 218 (2019).
40. T. Moriya *et al*., High-resolution single particle analysis from electron cryo-microscopy images using SPHIRE. *J. Vis. Exp.*, 55448 (2017).
41. F. J. O'Reilly, J. Rappsilber, Cross-linking mass spectrometry: Methods and applications in structural, molecular and systems biology. *Nat. Struct. Mol. Biol.* **25**, 1000–1008 (2018).
42. W. Girzalsky *et al*., Pex19p-dependent targeting of Pex17p, a peripheral component of the peroxisomal protein import machinery. *J. Biol. Chem.* **281**, 19417–19425 (2006).
43. J.-R. Su, K. Takeda, S. Tamura, Y. Fujiki, K. Miki, Crystal structure of the conserved N-terminal domain of the peroxisomal matrix protein import receptor, Pex14p. *Proc. Natl. Acad. Sci. U.S.A.* **106**, 417–421 (2009).
44. L.-A. Brown, A. Baker, Shuttles and cycles: Transport of proteins into the peroxisome matrix (review). (review). *Mol. Membr. Biol.* **25**, 363–375 (2008).
45. C. Brocard, G. Lametschwandtner, R. Koudelka, A. Hartig, Pex14p is a member of the protein linkage map of Pex5p. *EMBO J.* **16**, 5491–5500 (1997).
46. N. Shimizu *et al*., The peroxin Pex14p. cDNA cloning by functional complementation on a Chinese hamster ovary cell mutant, characterization, and functional analysis. *J. Biol. Chem.* **274**, 12593–12604 (1999).
47. W. B. Snyder *et al*., Pex17p is required for import of both peroxisome membrane and lumenal proteins and interacts with Pex19p and the peroxisome targeting signal-receptor docking complex in Pichia pastoris. *Mol. Biol. Cell* **10**, 4005–4019 (1999).
48. C. Holroyd, R. Erdmann, Protein translocation machineries of peroxisomes. *FEBS Lett.* **501**, 6–10 (2001).
49. C. Ma, S. Subramani, Peroxisome matrix and membrane protein biogenesis. *IUBMB Life* **61**, 713–722 (2009).
50. M. E. Oliveira, A. M. Gouveia, R. A. Pinto, C. Sá-Miranda, J. E. Azevedo, The energetics of Pex5p-mediated peroxisomal protein import. *J. Biol. Chem.* **278**, 39483–39488 (2003).
51. G. K. Will *et al*., Identification and characterization of the human orthologue of yeast Pex14p. *Mol. Cell. Biol.* **19**, 2265–2277 (1999).
52. J. S. Martenson *et al*, The importomer is a peroxisomal membrane protein translocase. *bioRxiv*:1863:2020.05.01.072660 (Posted 3 May 2020).
53. R. Erdmann, W. Schliebs, Peroxisomal matrix protein import: The transient pore model. *Nat. Rev. Mol. Cell Biol.* **6**, 738–742 (2005).
54. F. A. Salomons, J. A. Kiel, K. N. Faber, M. Veenhuis, I. J. van der Klei, Overproduction of Pex5p stimulates import of alcohol oxidase and dihydroxyacetone synthase in a Hansenula polymorpha Pex14 null mutant. *J. Biol. Chem.* **275**, 12603–12611 (2000).
55. D. Kerssen *et al*., Membrane association of the cycling peroxisome import receptor Pex5p. *J. Biol. Chem.* **281**, 27003–27015 (2006).
56. Y. Perez-Riverol *et al*., The PRIDE database and related tools and resources in 2019: Improving support for quantification data. *Nucleic Acids Res.* **47**, D442–D450 (2019).
57. J. Yang *et al*., Improved protein structure prediction using predicted interresidue orientations. *Proc. Natl. Acad. Sci. U.S.A.* **117**, 1496–1503 (2020).